Vol. 17, No. 3 (2018) 1121-1134
Revista Mexicana de Ingeniería Química

CYCLIC BIOSORPTION AND DESORPTION OF ACID RED 27 ONTO *Eichhornia crassipes* LEAVES

BIOSORCIÓN Y DESORCIÓN CÍCLICA DEL ROJO ÁCIDO 27 EN LAS HOJAS DE *Eichhornia crassipes*

A.E. Ramírez-Rodríguez, J.L. Reyes-Ledezma, G.M. Chávez-Camarillo, E. Cristiani-Urbina, L. Morales-Barrera*
Instituto Politécnico Nacional, Escuela Nacional de Ciencias Biológicas, Departamento de Ingeniería Bioquímica, Avenida Wilfrido Massieu s/n, Colonia Unidad Profesional Adolfo López Mateos, Delegación Gustavo A. Madero, Ciudad de México, 07738, México

Received: December 19, 2017; Accepted: February 28, 2018

Abstract

Eichhornia crassipes leaves (LEC) have been shown to be a highly effective biosorbent for the toxic dye Acid Red 27 (AR27). For continuous application, LEC biosorbent must be regenerated with a suitable desorption agent. The recovery of bound AR27 and the subsequent reuse of LEC were investigated in the present work over seven AR27 biosorption-desorption cycles. Desorption studies showed that the LEC-biosorbed dye could be effectively desorbed (100% efficiency) using dilute $NaHCO_3$ solution (0.025 M). Moreover, the biosorbent could be used effectively for at least seven biosorption-desorption cycles without any apparent physical change or damage and with undiminished AR27 biosorption capacity. The AR27 biosorption kinetics was well described by a pseudo-second-order model, whereas a pseudo-first-order model best described the AR27 desorption kinetics. Thus, LEC exhibits remarkable potential for application in detoxification of AR27-contaminated aqueous solutions.

Keywords: acid red 27 dye, biosorption, desorption, *Eichhornia crassipes*, biosorbent regeneration.

Resumen

Se ha demostrado que las hojas de *Eichhornia crassipes* (LEC) son un biosorbente altamente efectivo para el colorante tóxico Rojo Ácido 27 (AR27). Para una aplicación continua, el biosorbente LEC debe regenerarse con un agente desorbente adecuado. La recuperación del AR27 retenido y la posterior reutilización de LEC se investigaron en el presente trabajo por siete ciclos de biosorción-desorción de AR27. Los estudios de desorción mostraron que el colorante biosorbido en LEC podría desorberse de forma efectiva (100% de eficiencia) usando una solución diluida de $NaHCO_3$ (0.025 M). Además, el biosorbente podría usarse de manera efectiva durante al menos siete ciclos de biosorción-desorción sin ningún cambio o daño físico aparente y con una capacidad de biosorción de AR27 no disminuida. Las cinéticas de biosorción de AR27 fueron bien descritas por un modelo de pseudo-segundo orden, mientras que un modelo de pseudo-primer orden describió mejor las cinéticas de desorción de AR27. Por lo tanto, LEC exhibe un potencial notable para su aplicación en la desintoxicación de soluciones acuosas contaminadas con AR27.

Palabras clave: colorante rojo ácido 27, biosorción, desorción, *Eichhornia crassipes*, regeneración del biosorbente.

1 Introduction

Acid Red 27 (AR27) dye, also known as Amaranth, C.I. Food Red 9, E123, FD & C Red 2, Azorubin S, or C.I. 16185, is a sulfonated monoazo compound, which is widely used industrially for coloring foods, drinks, drugs, cosmetics, textiles, leather, paper, wood, and phenol-formaldehyde resins (Shabbir *et al*., 2017). As a consequence, these industries generate substantial amounts of wastewater colored with AR27. However, AR27 can have serious adverse effects on human health, causing allergies, respiratory problems, tumors, and birth defects owing to its cytotoxicity, cytostaticity, mutagenicity, carcinogenicity, and genotoxicity (Gupta *et al*., 2012). In addition, AR27 is considered to be an endocrine disrupter (Shabbir *et al*., 2017).

* *Corresponding author. E-mail*: lilianamor@prodigy.net.mx
doi: 10.24275/uam/izt/dcbi/revmexingquim/2018v17n3/Ramirez
issn-e: 2395-8472

Therefore, discharge of AR27-contaminated industrial wastewater into bodies of water poses a tremendous threat to human beings, as well as to aquatic flora and fauna. Most conventional treatment technologies cannot completely remove AR27 from contaminated water owing to its high solubility and stability in water and recalcitrance to biodegradation; in addition, such technologies are not cost-effective (Gupta *et al*., 2012; Shabbir *et al*., 2017). Biosorption has great potential to replace conventional methods for the removal of dyes owing to its environmental friendliness, enhanced efficiency, cost-effectiveness, minimization of secondary wastes, ease of operation, versatility, and simplicity of design (Asgher and Bhatti, 2010; Corral-Escárcega *et al*., 2017).

In this context, recent studies have demonstrated the high effectiveness of *Eichhornia crassipes* leaves (LEC), a biomass that is largely available worldwide, for biosorbing AR27 from aqueous solutions, confirmed by its high AR27 biosorption capacity (Guerrero-Coronilla *et al*., 2015). However, the successful application of any biosorbent depends not only on its biosorptive capacity, but also on the ease of dye desorption and biosorbent regeneration (Bessaha *et al*., 2016). To achieve effective reuse of a biosorbent, the desorption process should be cheap, nonpolluting, and regenerate the biosorbent in a state similar to its initial state, without any physical changes or damage and with undiminished dye biosorption capacity (Filipkowska, 2008).

Therefore, to develop an effective batch biosorption-desorption process and improve cost-effectiveness by recycling the biosorbent in multiple cycles, it is crucial to describe the biosorbent regeneration process (Szygula *et al*., 2008). In the present work, AR27 desorption from AR27-loaded LEC and regeneration of the biosorbent were studied. Several desorption solutions were examined and the influence of concentration on AR27 desorption was determined for the best solution.

The feasibility of regenerating LEC was investigated through seven consecutive biosorption-desorption cycles. Furthermore, the kinetics of the AR27 biosorption and desorption processes were analyzed using five different models, and the parameters of the kinetic models were obtained, which are key elements for designing biosorption and desorption biotechnological processes.

2 Materials and methods

2.1 Biosorbent preparation

Eichhornia crassipes plants were collected from the Xochimilco channels in Mexico City. The leaves were cut off, separated from the plants, washed thoroughly with distilled deionized water, and then oven-dried at 60 °C until a constant dry weight was obtained. Afterwards, the leaves were milled and sieved to obtain fractions with different particle sizes. The fraction with particle sizes of 0.15-0.30 mm was used in this study and designated as LEC. LEC was kept in an airtight plastic container until used.

2.2 AR27 solution

An AR27 (Sigma-Aldrich; 95% purity) solution was prepared at a concentration of 175 mg L^{-1} and pH 2.0 ± 0.1. The AR27 concentration was quantified spectrophotometrically (Genesys 10 UV/VIS, Thermo Electron Scientific Instruments Corporation) at a wavelength of 520 nm (Guerrero-Coronilla *et al*., 2014).

2.3 Desorption studies

LEC samples (at a concentration of 1 g L^{-1}) were mixed with a 175 mg L^{-1} AR27 solution at pH 2.0 ± 0.1 and 18 °C with constant agitation at 140 rpm for 24 h to ensure AR27 biosorption equilibrium was reached (Guerrero-Coronilla *et al*., 2015). Afterwards, AR27-loaded LEC was separated from the solution by centrifugation at 3000 rpm for 5 min, and the concentration of residual AR27 in the supernatant was determined to calculate the amount of AR27 biosorbed on the biosorbent. The amount of AR27 biosorbed per unit mass (dry weight) of LEC under equilibrium conditions was calculated according to the following mass balance equation (Guerrero-Coronilla *et al*., 2015):

$$q_e = \frac{c_e - c_0}{W} \tag{1}$$

where q_e is the AR27 biosorption capacity at equilibrium (mg g^{-1}), c_0 is the initial concentration of AR27 in the aqueous phase (mg L^{-1}), c_e is the equilibrium concentration of AR27 in solution (mg L^{-1}), and W is the LEC concentration (g L^{-1}).

The experimental equilibrium biosorption capacity of AR27 was found to be 61.54 mg g^{-1}, which is very close to that previously reported by Guerrero-Coronilla *et al*. (2015).

Subsequently, the pellets were washed thoroughly with distilled deionized water to remove any unbound dye. After centrifuging the resulting suspensions, the obtained AR27-loaded LEC was oven-dried at 60 °C until a constant dry weight was obtained. AR27-loaded LEC was stored in an airtight plastic container until further use.

In a preliminary AR27 desorption study, Guerrero-Coronilla *et al*. (2015) reported that neutral salt and acid desorption solutions have little or no positive effect on AR27 desorption, whereas alkaline solutions could achieve separation of AR27 from AR27-loaded LEC. Thus, in the present study, the effects of three common inorganic alkaline solutions (0.1 M NaOH, KOH, and $NaHCO_3$) and two organic solvent solutions (1% v/v acetone and chloroform) on AR27 desorption from AR27-loaded LEC were assessed. Each experiment was performed in a 500 mL Erlenmeyer flask containing 120 mL of desorption solution and 1 g (dry weight) of AR27-loaded LEC. The flask was agitated constantly in a shaker at 140 rpm, and samples were collected at different contact times. The collected samples were centrifuged at 3000 rpm for 5 min, and the supernatant was analyzed to quantify the AR27 concentration. After choosing the best chemical agent for desorption of AR27, experiments were performed to determine its optimal concentration (0.025, 0.05, and 0.1 M).

The AR27 desorption performance was evaluated using the desorption efficiency (E_{Dt}) and desorption capacity or desorption yield (Y_{Dt}), which can be calculated as follows (Filipkowska, 2008):

$$E_{Dt}(\%) = \frac{c_{Dt}}{q_e W} 100 \tag{2}$$

$$Y_{Dt} = \frac{c_{Dt} - c_{D0}}{W} \tag{3}$$

where c_{D0} and c_{Dt} are the initial and residual AR27 concentrations (mg L^{-1}) in the desorption solution at desorption time $t_D = 0$ min and $t_D = t_D$, respectively, and q_e is the AR27 concentration in the AR27-loaded LEC (mg g^{-1}) at time $t_D = 0$ min (AR27 biosorption capacity at equilibrium). The AR27 desorption efficiency (E_{De}) and capacity (Y_{De}) at equilibrium were calculated using eqs. (2) and (3), respectively, by replacing c_{Dt} with c_{De}, where c_{De} is the equilibrium concentration of AR27 in the desorption solution (mg L^{-1}).

2.4 Cyclic biosorption and desorption of AR27

Batch kinetic experiments for both biosorption and desorption of AR27 were performed. Studies on AR27 biosorption were carried out by agitating 120 mL of 175 mg L^{-1} AR27 solution and 1 g L^{-1} of LEC in 500 mL Erlenmeyer flasks at 140 rpm and 18 °C. Throughout the course of the biosorption experiments, the pH of the AR27 solution was kept constant at 2.0 ± 0.1 by periodic checking and adjusting with 0.1 M HCl or NaOH solutions when necessary (Guerrero-Coronilla *et al*., 2015).

Samples collected at various times were centrifuged at 3000 rpm for 5 min. Each supernatant was analyzed to determine the AR27 concentration, which was used to estimate the AR27 biosorption capacity at different experimental times using eq. (1), with q_e and c_e replaced by q_t and C_t, respectively, where q_t and c_t are the AR27 biosorption capacity and the residual AR27 concentration in solution at time $t = t$, respectively.

To check for glass sorption of AR27 and/or AR27 precipitation, LEC-free controls were run simultaneously under exactly the same conditions. No measurable changes were detected in AR27 concentration in the LEC-free controls, which indicates that the observed AR27 removal in the experiments with LEC was only due to the biosorbent. Prior to desorption of the dye from AR27-loaded LEC, the obtained pellets were washed thoroughly with distilled deionized water to remove unbound dye, and then oven-dried at 60 °C for 24 h.

Desorption of biosorbed AR27 from AR27-loaded LEC was carried out by agitating 120 mL of the desorption solution with 1 g L^{-1} AR27-loaded LEC in 500 mL Erlenmeyer flasks. At different desorption times, liquid samples were removed, centrifuged at 3000 rpm for 5 min, and used to determine the AR27 concentration. After the desorption step, the desorbed biosorbent was carefully washed with distilled deionized water to remove the desorption solution, oven-dried at 60 °C for 24 h, and then reused in the next biosorption step (second cycle). A total of seven cycles consisting of 7 h biosorption and 2 h desorption were conducted. During every biosorption-desorption cycle, samples of AR27-loaded and desorbed biosorbent were collected and analyzed using Fourier transform infrared (FTIR) spectroscopy and scanning electron microscopy (SEM).

Table 1. Biosorption and desorption kinetic models.

	Desorption		Biosorption	
Model				
Pseudo-first-order	$\ln Y_{Dt} = \ln Y_{De1} - k_{D1}t$ (Ho and McKay, 1999)	Y_{Dt}: desorption capacity at time t (mg g^{-1}) Y_{De1}: equilibrium desorption capacity predicted by the model (mg g^{-1}) k_{D1}: pseudo-first-order desorption rate constant (min^{-1})	$\ln q_t = \ln q_{e1} - k_1 t$ (Aşçi *et al.*, 2012)	q_t: biosorption capacity at time t (mg g^{-1}) q_{e1}: equilibrium biosorption capacity predicted by the model (mg g^{-1}) k_1: pseudo-first-order biosorption rate constant (min^{-1})
Pseudo-second -order	$Y_{Dt} = \frac{t}{\frac{1}{k_{D2}Y_{De2}^2} + \frac{t}{Y_{De2}}}$ (Ho and McKay, 1999)	Y_{De2}: equilibrium desorption capacity predicted by the model (mg g^{-1}) k_{D2}: pseudo-second-order desorption rate constant (min^{-1})	$q_t = \frac{t}{\frac{1}{k_2 q_{e2}^2} + \frac{t}{q_{e2}}}$ (Ho and McKay, 1999)	q_{e2}: equilibrium biosorption capacity predicted by the model (mg g^{-1}) k_2: pseudo-second-order biosorption rate constant (min^{-1})
Elovich	$Y_{Dt} = \frac{1}{\beta_D}\ln\alpha_D\beta_D + \frac{1}{\beta_D}\ln t$ (Wambu *et al.*, 2009)	α_D: initial rate of desorption (mg g^{-1} min^{-1}) β_D: desorption constant (g mg^{-1})	$q_t = \frac{1}{\beta}\ln\alpha\beta + \frac{1}{\beta}\ln t$ (Wambu *et al.*, 2009)	α: initial rate of biosorption (mg g^{-1} min^{-1}) β: bisorption constant (g mg^{-1})
Fractional power	$Y_{Dt} = k_{pD}t^{\nu D}$ (Hossain *et al.*, 2012)	νD: rate constant of desorption (min^{-1}) k_{pD}: model constant (mg g^{-1} min$^{-\nu D}$)	$q_t = k_p t^{\nu}$ (Hossain *et al.*, 2012)	ν: rate constant of biosorption (min^{-1}) k_p: model constant (mg g^{-1} min$^{-\nu}$)
Parabolic diffusion	$Y_{Dt} = Y_{D0} + k_{D0}t^{0.5}$ (Wambu *et al.*, 2009)	Y_{DO}: model constant (mg g^{-1}) k_{DO}: diffusion rate constant (mg g^{-1} min$^{-0.5}$)	$q_t + q_0 + q_0 t^{0.5}$ (Wambu *et al.*, 2009)	q_0: model constant (mg g^{-1}) k_0: diffusion rate constant (mg g^{-1} min$^{-0.5}$)

2.5 *FTIR spectroscopic analysis*

Samples of AR27-unloaded LEC (native LEC), as well as samples of AR27-loaded and AR27-desorbed LEC from each biosorption-desorption cycle, were oven-dried at 105 °C for 24 h. Then, each sample was finely ground, mixed with dried spectroscopic KBr in a 1:5 ratio, and then immediately analyzed with a Perkin-Elmer Spectrum 2000 FTIR spectrophotometer equipped with a Perkin-Elmer diffuse reflectance FTIR accessory. FTIR spectra were obtained using 16 scans over range of 4000-400 cm^{-1} with a resolution of 4 cm^{-1}.

2.6 *SEM analysis*

To examine the morphological and surface characteristics of native LEC, as well as those of AR27-loaded and AR27-desorbed biosorbents from the first and seventh biosorption-desorption cycles, micrographs of dried native, AR27-loaded, and desorbed biosorbents were obtained at a magnification of ×1000 using a high resolution scanning electron microscope (JSM7800F, JEOL) at an accelerating voltage of 15 kV after carbon coating.

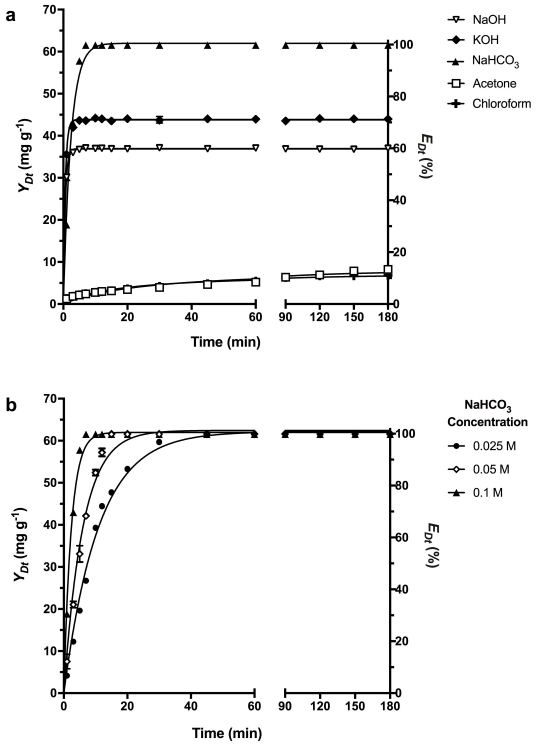

Fig. 1. Effect of desorption solution (a) and $NaHCO_3$ concentration (b) on AR27 desorption capacity (Y_{Dt}) and efficiency (E_{Dt}) (−, Pseudo-first-order model prediction).

2.7 Modeling of biosorption and desorption kinetics

Information on the kinetics of solute biosorption and desorption is crucial for designing effective biosorption and desorption systems, and selecting optimum operating conditions for full-scale batch biosorption and desorption systems (Aşçi *et al*., 2012). Desorption kinetics is also important for the regeneration of the biosorbent and recovery of the adsorbate, making the treatment process more economical (Mahmoodi *et al*., 2011). In the present work, the kinetics of the AR27 biosorption and desorption processes were analyzed using pseudo-first-order, pseudo-second-order, Elovich, fractional power, and parabolic diffusion models (Table 1).

2.8 Statistical and data analysis

Three independent replicates confirmed that the AR27 biosorption and desorption experiments were reproducible within an error of 5%, and mean values are reported herein. AR27 biosorption and desorption data were statistically analyzed by two-way analysis of variance (ANOVA) with Tukey's test (overall confidence level = 0.05) using GraphPad Prism software version 7.0 (GraphPad Software, Inc.).

All of the parameters in the biosorption and desorption kinetic models were evaluated by nonlinear regression analysis of the experimental data using GraphPad Prism software version 7.0 (GraphPad Software, Inc.). The best-fit models were selected by the highest coefficient of determination (R^2), the lowest residual or sum of squares error (SSE) and root mean squared error or standard error (RMSE) values, and the narrowest 95% confidence intervals.

3 Results and discussion

3.1 Effect of desorption solution on AR27 desorption kinetics

In the present work, five potential desorption solutions were assayed for their ability to desorb AR27 from AR27-loaded LEC. Fig. 1a displays the AR27 desorption capacity (Y_{Dt}) and AR27 desorption efficiency (E_{Dt}) as a function of desorption time for the five desorption solutions. The longest and the least effective desorption processes were observed when organic solvent solutions (1% v/v acetone and chloroform) were used. After 180 min of desorption, the AR27 desorption capacities and efficiencies obtained with 1% v/v acetone and chloroform solutions were similar, with values of 6.4 and 7.7 mg g^{-1} and 10.4 and 12.5%, respectively (Fig. 1a). In contrast, it is evident from Fig. 1a that with the assayed alkaline desorption solutions (0.1 M NaOH, KOH, and $NaHCO_3$), AR27 desorption was very fast initially, becoming slower towards equilibrium. All AR27 was desorbed (100% desorption efficiency) from AR27-loaded LEC with 0.1 M $NaHCO_3$ after only 7 min, whereas about 71.29% and 59.86% of AR27 was desorbed with 0.1 M KOH and NaOH, respectively. The release of AR27 from the AR27-loaded LEC biomass with aqueous alkaline solutions was easy and opposite to that of pH effect on AR27 biosorption (Guerrero-Coronilla *et al*., 2015).

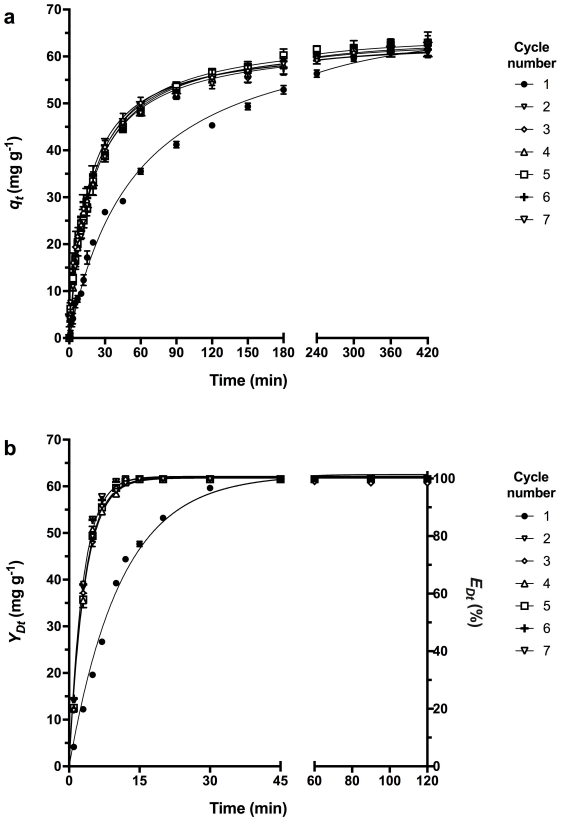

Fig. 2. Kinetics of AR27 biosorption onto LEC (a) and AR27 desorption from AR27-loaded LEC (b) over seven cycles (–: (a) Pseudo-second-order model prediction; (b) Pseudo-first-order model prediction)

Table 2. Parameters of kinetic models for AR27 desorption from AR27-loaded LEC with different $NaHCO_3$ concentrations.

	0.025M	**0.05M**	**0.1M**
		Experimental data	
E_{Dmax} (%)	100 ± 0.001	100 ± 0.001	100 ± 0.001
Y_{De} (mg g^{-1})	61.54 ± 0.001	61.54 ± 0.001	61.54 ± 0.001
		Pseudo-first-order	
Y_{De1} **(mg g^{-1})**	62.47 ± 0.467	62.45 ± 0.385	61.98 ± 0.216
k_{D1} **(min^{-1})**	0.091 ± 0.002	0.1663 ± 0.004	0.423 ± 0.010
R^2	0.991	0.984	0.984
SSE	181	267.2	118.9
RMSE	1.903	2.146	1.432
		Pseudo-second-order	
Y_{De2} **(mg g^{-1})**	71.54 ± 1.461	66.950 ± 1.111	64.880 ± 0.755
k_{D2} **(g mg^{-1} min^{-1})**	0.002 ± 0.0001	0.004 ± 0.001	0.012 ± 0.001
R^2	0.961	0.918	0.871
SSE	794.8	1392	979
RMSE	3.987	4.898	4.108
		Elovich	
β_D **(g mg^{-1})**	0.071 ± 0.003	0.103 ± 0.008	0.190 ± 0.026
α_D **(mg g^{-1} min^{-1})**	18.38 ± 1.958	88.47 ± 32.17	12575 ± 17121
R^2	0.0911	0.727	0.479
SSE	1796	4621	3962
RMSE	5.993	8.926	8.266
		Fractional power	
k_{pD} **(mg g^{-1} $min^{-\nu D}$)**	17.73 ± 1.702	30.14 ± 2.347	44.19 ± 2.261
ν_D	0.295 ± 0.025	0.165 ± 0.020	0.082 ± 0.014
R^2	0.798	0.616	0.420
SSE	4091	6498	4414
RMSE	9.046	10.58	8.724
		Parabolic diffusion	
Y_{DO} **(mg g^{-1})**	15.29 ± 2.902	34.34 ± 3.045	49.27 ± 2.396
k_{DO} **(mg g^{-1} $min^{-0.5}$)**	5.626 ± 0.512	2.844 ± 0.431	1.342 ± 0.339
R^2	0.707	0.429	0.212
SSE	5926	9682	5994
RMSE	10.89	12.92	10.17

The biosorption of AR27 in an acidic medium and desorption in an alkaline medium indicates that the ion exchange might be the major mechanism of AR27 biosorption and desorption. It is well known that when a sorbate binds to a biosorbent by ion exchange, even a small change in the solution pH can bring about an effective release of the sequestered sorbate (Volesky, 2003). Thus, if acid or alkaline solutions desorb a dye, then biosorption and desorption occur by ion exchange (Gad and El-Sayed, 2009). The above results clearly indicate that $NaHCO_3$ solution is the best eluent for AR27 desorption from AR27-loaded LEC and consequently, further studies were conducted using $NaHCO_3$ solution to desorb AR27 from AR27-loaded LEC. To the best of our knowledge, the effective performance of $NaHCO_3$ for AR27 desorption has not been reported elsewhere.

3.2 Effect of $NaHCO_3$ concentration on desorption capacity and efficiency

Fig. 1b shows the kinetic profiles of AR27 desorption capacity (Y_{Dt}) and efficiency (E_{Dt}) for $NaHCO_3$ desorption solution with different concentrations. It should be noted that, regardless of $NaHCO_3$ concentration, rapid AR27 desorption was observed initially, with the rate gradually diminishing until the AR27 desorption capacity and efficiency reached maximum constant values corresponding to the equilibrium desorption capacity (61.54 mg g^{-1}) and efficiency (100%). However, the time required to reach equilibrium decreased with increasing $NaHCO_3$ concentration (Fig. 1b).

Furthermore, the kinetic profiles of AR27 desorption were mathematically modeled to determine the rate-controlling mechanisms involved in the desorption process. For this purpose, pseudo-first-order, pseudo-second-order, Elovich, fractional power, and parabolic diffusion models were used to analyze the experimental desorption data at different $NaHCO_3$ concentrations. Table 2 lists the experimental equilibrium desorption capacity (Y_{De}) and maximum desorption efficiency (E_{Dmax}), as well as the parameters determined for the pseudo-first-order (Y_{De1}, k_{D1}), pseudo-second-order (Y_{De2}, k_{D2}), Elovich (α_D, β_D), fractional power (k_{pD}, ν_D), and parabolic diffusion (Y_{DO}, k_{DO}) kinetic models for AR27 desorption at $NaHCO_3$ concentrations from 0.025 to 0.1 M, together with the corresponding R^2, SSE, RMSE, and 95% confidence interval values.

The determination coefficients were higher with the pseudo-first-order model, and the SSE and RMSE values were lower than those obtained with the pseudo-second-order, Elovich, fractional power, and parabolic diffusion models, which denotes good agreement between the experimental data and the pseudo-first-order model for the assayed concentrations of $NaHCO_3$ in the desorption solution. Indeed, as shown by the continuous lines in Fig. 1b, the pseudo-first-order model successfully describes the kinetic profiles of AR27 desorption from AR27-loaded LEC at all assayed concentrations of the desorption solution. Furthermore, the equilibrium desorption capacity (Y_{De1}) values predicted by the pseudo-first-order model agrees very well with the experimental desorption data (Y_{De}). Therefore, the pseudo-first-order model was chosen as the most suitable for describing AR27 desorption kinetics, which implies that the rate-controlling step in the desorption process may be chemical in nature.

The rate constant (k_{D1}) of the pseudo-first-order model was observed to increase as the desorption solution concentration increased, which confirms that AR27 desorption is faster and equilibrium is reached more rapidly at higher desorption solution concentrations. However, higher $NaHCO_3$ concentrations (0.05 and 0.1 M) may damage the LEC structure and reduce the capacity of AR27 biosorption and desorption by LEC biomass loss, impairing reuse of the biosorbent in subsequent biosorption-desorption cycles. Moreover, the lower $NaHCO_3$ concentration (0.025 M) yielded an AR27 desorption efficiency (100%) and equilibrium desorption capacity (61.54 mg g^{-1}) equal to those obtained with higher $NaHCO_3$ concentrations (0.05 and 0.1 M) in a relatively short desorption time (45 min).

Further, the cost of the AR27 desorption process would be lower if a lower concentration of desorption agent were used. Therefore, it is reasonable to choose 0.025 M $NaHCO_3$ for AR27 desorption from AR27-loaded LEC, and all further desorption studies were performed using 0.025 M $NaHCO_3$.

3.3 Cyclical AR27 biosorption and desorption kinetics

To investigate the regeneration ability of the LEC biosorbent, seven sequential biosorption-desorption cycles were carried out using the same biosorbent. Figs. 2a and 2b show the kinetic profiles of AR27 biosorption by LEC and AR27 desorption from AR27-loaded LEC, respectively, for each cycle. In each cycle, the biosorption and desorption capacities of AR27 gradually rose with time, reaching maximum constant values that corresponded to the equilibrium biosorption ($q_{e\,exp}$) and desorption capacity (Y_{De}) values. Furthermore, the rates of the biosorption and desorption processes were fast during the first few minutes, and then decreased gradually until the dynamic equilibria of AR27 biosorption and desorption were reached.

No significant differences were found in the experimental equilibrium biosorption capacities of AR27 (60.82-62.37 mg g^{-1}; Fig. 2a and Table 3), the experimental equilibrium desorption capacities (61.24-61.54 mg g^{-1}; Fig. 2b and Table 4), or the AR27 desorption efficiencies at equilibrium (99.51-100%; Fig. 2b and Table 4) of the seven cycles. However, the rates of biosorption and desorption of AR27 for the first cycle were significantly lower than those of the remaining biosorption and desorption cycles (Figs. 2a and 2b).

Table 3. Parameters of kinetic models for AR27 biosorption by LEC for each cycle.

	Cycle number						
	1	**2**	**3**	**4**	**5**	**6**	**7**
$q_{e\ exp}$ (**mg g^{-1}**)	61.21 ± 0.839	61.4 ± 0.7857	61.98 ± 0.635	62.37 ± 0.487	62.14 ± 0.361	60.86 ± 0.313	60.82 ± 0.262
Pseudo-first-order							
q_{e1} (**mg g^{-1}**)	58.4 ± 0.595	57.48 ± 0.498	57.42 ± 0.604	57.94 ± 0.517	57.94 ± 0.537	57.46 ± 0.507	58.39 ± 0.465
k_1 (**min^{-1}**)	0.016 ± 0.001	0.043 ± 0.001	0.049 ± 0.002	0.045 ± 0.002	0.042 ± 0.001	0.050 ± 0.002	0.0451 ± 0.001
R^2	0.981	0.970	0.952	0.969	0.967	0.967	0.976
SSE	1077	1417	2193	1553	1642	1548	1216
RMSE	3.021	3.465	4.311	3.628	3.73	3.622	3.21
Pseudo-second-order							
q_{e2} (**mg g^{-1}**)	69.46 ± 0.531	63.6 ± 0.307	62.96 ± 0.482	64.04 ± 0.338	65.05 ± 0.344	63.04 ± 0.313	64.57 ± 0.287
k_2 (**g mg^{-1} min^{-1}**)	3E-4 ± 1E-5	9E-4 ± 2E-5	1E-3 ± 1E-5	9E-4 ± 2E-5	9E-4 ± 2E-5	1E-3 ± 2E-5	8E-4 ± 2E-5
R^2	0.994	0.994	0.983	0.993	0.993	0.993	0.995
SSE	318.5	296.2	808.7	367.3	371.5	339.4	252.4
RMSE	1.643	1.584	2.618	1.764	1.774	1.696	1.462
Elovich							
β (**g mg^{-1}**)	0.084 ± 0.002	0.094 ± 0.001	0.097 ± 0.001	0.093 ± 0.001	0.092 ± 0.001	0.095 ± 0.001	0.092 ± 0.001
α (**mg g^{-1} min^{-1}**)	4.454 ± 0.212	12.1 ± 0.580	14.68 ± 0.752	11.97 ± 0.530	12.34 ± 0.563	13.69 ± 0.641	11.37 ± 0.554
R^2	0.957	0.976	0.976	0.979	0.979	0.979	0.974
SSE	2150	916.2	879.8	827	869.3	800.3	1051
RMSE	4.382	2.86	2.803	2.717	2.786	2.673	3.063
Fractional power							
k_p (**mg g^{-1} min$^{-\nu}$**)	5.854 ± 0.32	13.810 ± 0.59	15.250 ± 0.62	14.040 ± 0.63	14.150 ± 0.60	15.130 ± 0.68	13.710 ± 0.27
ν	0.409 ± 0.01	0.267 ± 0.008	0.251 ± 0.008	0.266 ± 0.009	0.267 ± 0.008	0.252 ± 0.009	0.654 ± 0.01
R^2	0.964	0.931	0.925	0.923	0.931	0.913	0.917
SSE	1832	2687	2754	3106	2810	3294	3391
RMSE	4.044	4.898	4.959	5.266	5.009	5.423	5.502
Parabolic diffusion							
q_0 (**mg g^{-1}**)	2.828 ± 0.72	14.14 ± 1.18	15.88 ± 1.22	14.31 ± 1.23	14.48 ± 1.21	15.65 ± 1.29	13.89 ± 1.26
k_0 (**mg g^{-1} min$^{-0.5}$**)	3.382 ± 0.07	2.952 ± 0.12	2.869 ± 0.12	2.988 ± 0.12	3.015 ± 0.12	2.882 ± 0.13	3.002 ± 0.12
R^2	0.951	0.847	0.829	0.837	0.846	0.814	0.833
SSE	2730	7307	7885	8044	7703	8806	8357
RMSE	4.81	7.869	8.174	8.256	8.079	8.639	8.416

This behavior could be attributed to the removal of some chemical compounds or impurities (which slow down the kinetics) from the LEC biomass surface during the first desorption step with $NaHCO_3$, resulting in increased AR27 biosorption and desorption rates in the remaining cycles. Similar behavior was reported by Lezcano *et al*. (2011), who investigated the effectiveness of biomass from an eutrophized ecosystem for two biosorption-desorption cycles of Cd and Cu using $NaHCO_3$ as a desorption agent.

Previous studies of successive biosorption and desorption of dyes have shown decreased dye biosorption and desorption capacities with increased cycling (Asgher and Bhatti, 2010; Bessaha *et al*., 2016; Filipkowska, 2008; Szygula *et al*., 2008). This decrease has been ascribed to the irreversible binding of dyes to the active sites in the biosorbents (Filipkowska, 2008) and/or the degradation of biosorbents under the extreme pH conditions used during the biosorption and desorption processes (Demarchi *et al*., 2015). Moreover, Rêgo *et al*. (2013) reported that chitosan films could only maintain the same physical adsorbent characteristics and biosorption capacity over two AR27 biosorption-desorption cycles. In the present work, no decrease was observed in the AR27 biosorption and desorption capacities and no biosorbent loss was detected over seven biosorption-desorption cycles, which makes LEC very suitable for designing a continuous batch reactor.

Furthermore, the effectiveness of cyclical AR27 biosorption and desorption was evaluated by modeling the kinetics of AR27 biosorption and desorption and determining the order of the reaction and the rate constants.

Table 4. Parameters of kinetic models for AR27 desorption from AR27-loaded LEC for each cycle.

	Cycle number						
	1	**2**	**3**	**4**	**5**	**6**	**7**
E_{Dmax} **(%)**	100 ± 0.001	100 ± 0.001	99.51 ± 0.69	99.85 ± 0.41	99.89 ± 0.302	99.89 ± 0.33	99.9 ± 0.32
Y_{De} **(mg g^{-1})**	61.54 ± 0.001	61.54 ± 0.001	61.24 ± 0.42	61.45 ± 0.25	61.47 ± 0.19	61.47 ± 0.20	61.48 ± 0.19
	Pseudo-first-order						
Y_{De1} **(mg g^{-1})**	62.47 ± 0.47	61.82 ± 0.26	61.74 ± 0.26	61.89 ± 0.26	62.02 ± 0.23	62.01 ± 0.22	62.07 ± 0.25
k_{D1} **(min^{-1})**	0.091 ± 0.002	0.310 ± 0.007	0.301 ± 0.007	0.297 ± 0.006	0.296 ± 0.006	0.339 ± 0.007	0.336 ± 0.007
R^2	0.991	0.989	0.990	0.990	0.992	0.991	0.989
SSE	181	106.6	103.6	104.3	80.99	79.73	103.6
RMSE	1.903	1.46	1.439	1.444	1.273	1.263	1.439
	Pseudo-second-order						
Y_{De2} **(mg g^{-1})**	71.54 ± 1.46	66.32 ± 0.93	66.14 ± 1.00	66.46 ± 0.95	66.54 ± 0.96	66.23 ± 0.93	66.33 ± 0.97
k_{D2} **(g mg^{-1} min^{-1})**	0.002 ± 1E-4	0.007 ± 7E-4	0.007 ± 8E-4	0.007 ± 7E-4	0.007 ± 7E-4	0.008 ± 8E-4	0.008 ± 9E-4
R^2	0.961	0.919	0.909	0.920	0.918	0.908	0.903
SSE	794.8	801.3	919.4	821.7	839.5	838.3	911.2
RMSE	3.987	4.003	4.288	4.054	4.097	4.095	4.269
	Elovich						
β_D **(g mg^{-1})**	0.071 ± 0.003	0.120 ± 0.012	0.120 ± 0.013	0.117 ± 0.012	0.117 ± 0.012	0.128 ± 0.014	0.127 ± 0.014
α_D **(mg g^{-1} min^{-1})**	18.38 ± 1.958	352.9 ± 206	352.1 ± 213.8	306.8 ± 170	316.5 ± 179.2	586.7 ± 407.3	554.3 ± 384.7
R^2	0.0911	0.652	0.634	0.661	0.656	0.616	0.611
SSE	1796	3462	3700	3464	3518	3510	3647
RMSE	5.993	8.321	8.603	8.323	8.388	8.378	8.54
	Fractional power						
k_{pD} **(mg g^{-1} min$^{-\nu D}$)**	17.73 ± 1.702	37.14 ± 2.43	37.05 ± 2.503	36.61 ± 2.428	36.77 ± 2.445	38.86 ± 2.446	38.75 ± 2.488
νD	0.295 ± 0.025	0.134 ± 0.02	0.133 ± 0.20	0.137 ± 0.02	0.136 ± 0.02	0.123 ± 0.02	0.124 ± 0.02
R^2	0.798	0.554	0.536	0.562	0.557	0.526	0.521
SSE	4091	4432	4690	4476	4527	4331	4494
RMSE	9.046	9.415	9.865	9.461	9.515	9.307	9.481
	Parabolic diffusion						
Y_{DO} **(mg g^{-1})**	15.29 ± 2.90	41.00 ± 3.05	41.00 ± 3.11	40.40 ± 3.06	40.60 ± 3.08	42.94 ± 2.99	42.83 ± 3.03
k_{DO} **(mg g^{-1} min$^{-0.5}$)**	5.626 ± 0.51	2.751 ± 0.54	2.697 ± 0.55	2.827 ± 0.54	2.807 ± 0.54	2.516 ± 0.53	2.533 ± 0.54
R^2	0.707	0.344	0.326	0.354	0.349	0.314	0.310
SSE	5926	6521	6822	6606	6663	6270	6470
RMSE	10.89	11.42	11.68	11.49	11.54	11.2	11.38

The parameters of the pseudo-first-order, pseudo-second-order, Elovich, fractional power, and parabolic diffusion models obtained from the AR27 biosorption and desorption kinetics are shown in Tables 3 and 4, respectively.

For each AR27 biosorption step, the pseudo-second-order model had higher determination coefficients and lower SSE and RMSE values than the pseudo-first-order, Elovich, fractional power, and parabolic diffusion kinetic models. Furthermore, the pseudo-second-order model described well the variations of AR27 biosorption capacity with time (continuous lines in Fig. 2a) and predicted biosorption capacity at equilibrium values (q_{e2}) that were very close to the experimentally obtained maximum capacities ($q_{e\,exp}$, Table 3). Thus, the biosorption of AR27 dye molecules by LEC followed a pseudo-second-order model. A pseudo-second-order has been previously found to be the most suitable model for describing the kinetic profiles of AR27 biosorption by LEC at different solution pH values, initial AR27 concentrations, and temperatures (Guerrero-Coronilla *et al.*, 2015). The rate constant of the pseudo-second-order model (k_2) for the first step of AR27 biosorption was lower than those for the six subsequent biosorption steps. In contrast, no significant differences were found between the k_2 values for the second to seventh steps of AR27 biosorption.

Furthermore, the pseudo-first-order model clearly yielded the highest R^2 and the lowest SSE and RMSE values of the five assayed kinetic models for each of the seven AR27 desorption steps. Indeed, the pseudo-first-order model successfully described the kinetic profiles of AR27 desorption (continuous lines in Fig. 2b), and the predicted AR27 desorption capacity

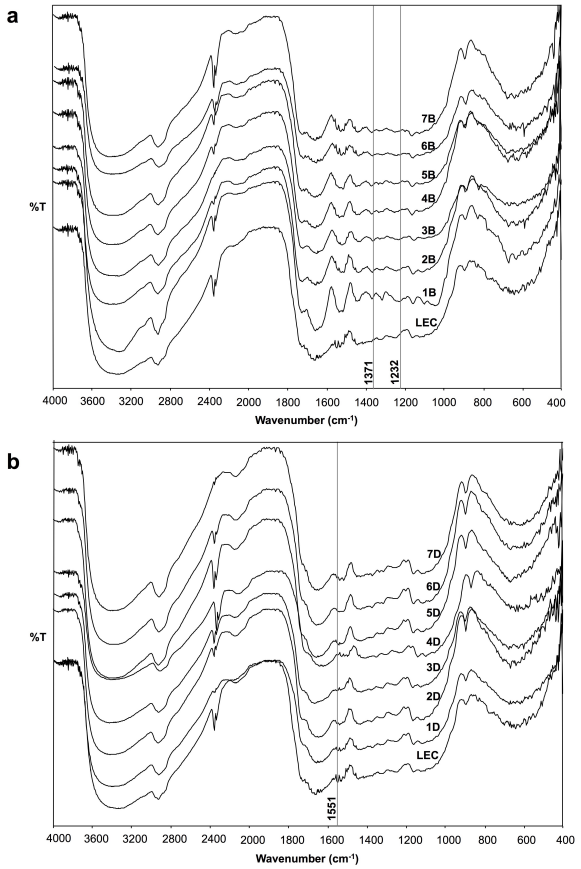

Fig. 3. Comparison of the FTIR spectrum of native LEC with the spectra of AR27-loaded LEC (a) and AR27-desorbed LEC (b) obtained after each biosorption-desorption cycle.

values at equilibrium (Y_{De1}) are very close to the capacities obtained experimentally (Y_{De}; Table 4). In addition, the rate constants of the pseudo-first-order model (k_{D1}) for the second and subsequent AR27 desorption steps were higher than that for the first desorption step.

The AR27 desorption process occurred much faster than the AR27 biosorption process, as evidenced experimentally and by the higher values of the rate constants of the pseudo-first-order and pseudo-second-order kinetic models. Furthermore, LEC biomass can be reused for at least seven biosorption-desorption cycles, which is expected to reduce significantly the cost of the AR27 treatment

3.4 FTIR studies

Previous FTIR studies conducted by our research group revealed that amide functional groups play a key role in the biosorption of AR27 by LEC (Guerrero-Coronilla *et al*., 2014). In the current study, FTIR spectroscopy was applied to confirm the presence and absence of AR27 functional groups on the biosorbent surface after each biosorption and desorption step over seven cycles.

Fig. 3 shows comparisons of the FTIR spectrum of native LEC with the spectra of AR27-loaded LEC (Fig. 3a) and AR27-desorbed LEC (Fig. 3b).

The FTIR spectra of AR27-loaded LEC shows absorption peaks at approximately 1371 and 1232 cm^{-1}, which are assigned to −S=O stretching of the naphthalene rings in AR27 (Ghodake *et al*., 2011) and the CH in-plane bending vibration of naphthalene rings (Snehalatha *et al*., 2008), respectively; in contrast, these absorption peaks are not found in the FTIR spectrum of native LEC. These results clearly confirm the biosorption of AR27 onto LEC. Another important change in the spectra on biosorption of AR27 is the disappearance of the peak associated with amide II N−H bending at approximately 1551cm^{-1} (Stuart, 2004), which corroborates that amide groups are involved in AR27 biosorption by LEC. In addition, the spectra of all the AR27-loaded samples are similar, which indicates that the chemical composition of the biosorbent did not change significantly after several biosorption-desorption cycles.

Compared with the FTIR spectra of AR27-loaded LEC, a peak at 1551cm^{-1} corresponding to the amide II functional group is observed in the spectra of the AR27-desorbed biosorbent samples, whereas peaks at 1371 and 1232cm^{-1} corresponding to the naphthalene rings of AR27 are not observed. Furthermore, no significant differences are detected between the spectrum of native LEC and the spectra of AR27-desorbed LEC. These findings indicate that all AR27 was desorbed from AR27-loaded LEC and that the amide functional groups were not affected by successive biosorption-desorption cycles.

3.5 SEM analysis

SEM has been widely used to study the morphological features, surface characteristics, and fundamental physical properties of biosorbent materials. It is also a useful tool to determine the shape of a biosorbent (Mahmoodi *et al*., 2011; Carreño-De León *et al*., 2017).

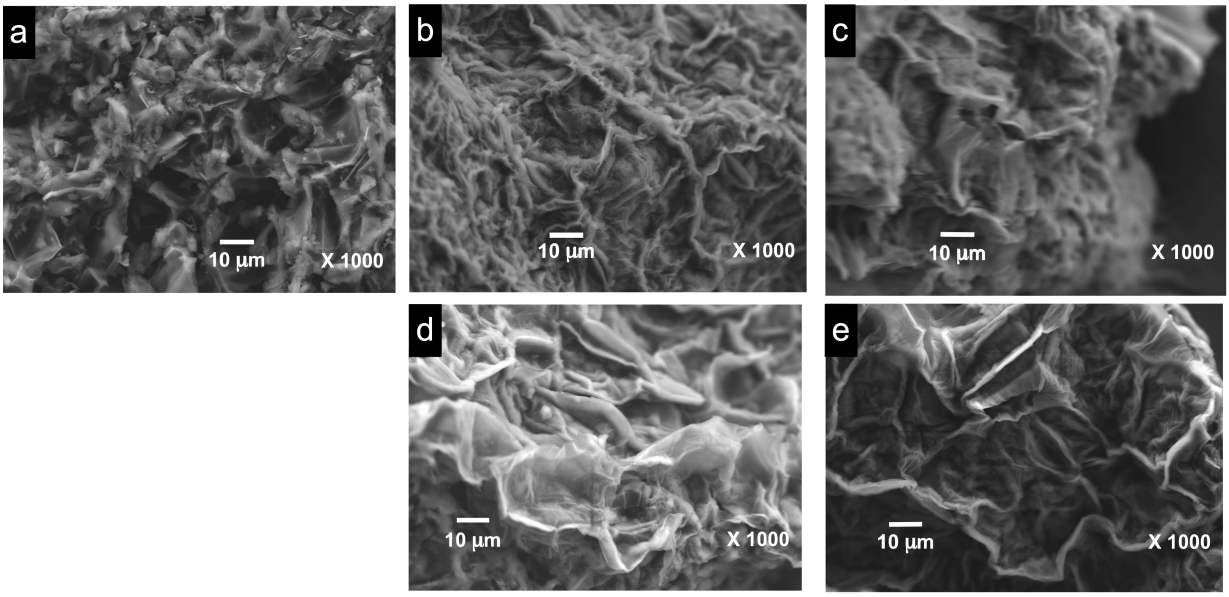

Fig. 4. SEM micrographs of native LEC (a), AR27-loaded LEC (b) and AR27-desorbed LEC (c) during the first biosorption-desorption cycle, and AR27-loaded LEC (d) and AR27-desorbed LEC (e) during the seventh biosorption-desorption cycle.

In this work, SEM analysis was performed at a magnification of ×1000 to evaluate possible damage to the biosorbent structure that might result from its use in successive biosorption-desorption cycles.

SEM micrographs reveal that native LEC has a rough and porous surface, with irregular pore structures (Fig. 4a), which makes biosorption of AR27 on different parts of the biosorbent possible. From the SEM images of the AR27-loaded and AR27-desorbed biosorbents after the first (figs. 4b and 4c) and seventh cycles of biosorption and desorption (figs. 4d and 4e), there is no evidence of damage to the biosorbent, which retained its microscopic and macroscopic appearance and surface integrity after seven cycles of AR27 biosorption-desorption. These findings agree with the results of the kinetic studies, which clearly showed that the biosorbent retained its performance for biosorbing and desorbing AR27 with repeated cycling.

Conclusions

This study showed that LEC can be used in biosorption and desorption cycles to treat AR27-contaminated aqueous solutions. The use of 0.025 M $NaHCO_3$ as a desorption agent does not affect the ability of LEC to biosorb AR27 nor does it damage the LEC structure, even after seven biosorption-desorption cycles. Thus, the LEC biosorbent does not need to be replaced after every biosorption step, which decreases process treatment costs. Furthermore, the short biosorption and desorption times increase the applicability of LEC for treating larger volumes of AR27-contaminated wastewater.

Acknowledgements

This work was supported by the Secretaría de Investigación y Posgrado, IPN. The CONACyT awarded a graduate scholarship to two of the co-authors (A.E.R.-R. and J.L.R.-L.). E.C.-U. is a holder of grants from COFAA-IPN, EDI-IPN and SNI-CONACyT. L.M.-B. is a holder of grants from EDI-IPN and SNI-CONACyT.

Nomenclature

AR27	Acid Red 27 dye
C_{D0}	initial AR27 concentration in the desorption solution at $t_D = 0$ min, mg L^{-1}
C_{De}	equilibrium concentration of AR27 in the desorption solution, mg L^{-1}

C_{Dt} residual AR27 concentration in the desorption solution at desorption time $t_D = t_D$, mg L^{-1}
C_e equilibrium concentration of AR27 in solution, mg L^{-1}
C_0 initial concentration of AR27 in the aqueous phase, mg L^{-1}
E_{De} AR27 desorption efficiency at equilibrium, %
E_{Dt} desorption efficiency, %
k_0 parabolic diffusion biosorption rate constant, mg g^{-1} $min^{-0.5}$
k_1 pseudo-first-order biosorption rate constant, min^{-1}
k_2 pseudo-second-order biosorption rate constant, min^{-1}
k_{D1} pseudo-first-order desorption rate constant, min^{-1}
k_{D2} pseudo-second-order desorption rate constant, min^{-1}
k_{DO} parabolic diffusion desorption rate constant, mg g^{-1} $min^{-0.5}$
k_p fractional power biosorption model constant, mg g^{-1} min^{-v}
k_{pD} fractional power desorption model constant, mg g^{-1} min^{-vD}
LEC *Eichhornia crassipes* leaves
q_0 parabolic diffusion model constant, mg g^{-1}
q_e AR27 biosorption capacity at equilibrium, mg g^{-1}
q_{e1} equilibrium biosorption capacity predicted by the pseudo-first-order model, mg g^{-1}
q_{e2} equilibrium biosorption capacity predicted by the pseudo-second-order model, mg g^{-1}
q_t biosorption capacity at time t, mg g^{-1}
R^2 coefficient of determination, -
RMSE root mean squared error or standard error, -
SSE residual or sum of squares error, -
t time, min
t_D desorption time, min
W LEC concentration, g L^{-1}
Y_{De} desorption capacity at equilibrium, mg g^{-1}
Y_{De1} equilibrium desorption capacity predicted by the pseudo-first-order model, mg g^{-1}
Y_{De2} equilibrium desorption capacity predicted by the pseudo-second-order model, mg g^{-1}
Y_{DO} parabolic diffusion model constant, mg g^{-1}
Y_{Dt} desorption capacity or desorption yield at time t, mg g^{-1}

Greek symbols

α initial rate of biosorption in Elovich model, mg g^{-1} min^{-1}
α_D initial rate of desorption in Elovich model, mg g^{-1} min^{-1}
β Elovich biosorption constant, g mg^{-1}
β_D Elovich desorption constant, g mg^{-1}
ν rate constant of biosorption in fractional power model, min^{-1}
ν_D rate constant of desorption in fractional power model, min^{-1}

References

Aşçi, Y., Açikel, Ü. and Sağ Açikel, Y. (2012). Equilibrium, hysteresis and kinetics of cadmium desorption from sodium-feldspar using rhamnolipid biosurfactant. *Environmental Technology 33*, 1857-1868.

Asgher, M. and Bhatti, H.N. (2010). Mechanistic and kinetic evaluation of biosorption of reactive azo dyes by free, immobilized and chemically treated *Citrus sinensis* waste

biomass. *Ecological Engineering 36*, 1660-1665.

Bessaha, F., Marouf-Khelifa, K., Batonneau-Gener, I. and Khelifa, A. (2016). Characterization and application of heat-treated and acid-leached halloysites in the removal of malachite green: adsorption, desorption, and regeneration studies. *Desalination and Water Treatment 57*, 14609-14621.

Carreño-De León, M.C., Solache-Ríos, M.J., Cosme-Torres, I., Hernandez-Berriel, M.C. and Flores-Alamo, N. (2017). Adsorption of Cr(VI) by *Zea mays* rachis. *Revista Mexicana de Ingeniería Química 16*, 261-269.

Corral-Escarcega, M.C., Ruiz-Gutierrez, M.G., Quintero-Ramos, A., Melendez-Pizarro, C.O., Lardizabal-Gutierrez, D. and Campos-Venegas, K. (2017). Use of biomass-derived from pecan nut husks (*Carya illinoinensis*) for chromium removal from aqueous solutions. Column modeling and adsorption kinetics studies. *Revista Mexicana de Ingeniería Química 16*, 939-953.

Demarchi, C.A., Debrassi, A., de Campos Buzzi, F., Nedelko, N., Slawska-Waniewska, A., Dłuzewski, P., Magro, J.D., Scapinello, J. and Rodrigues, C.A. (2015). Adsorption of the dye remazol red 198 (RR198) by *O*-carboxymethylchitosan-N-lauryl/γ-Fe_2O_3 magnetic nanoparticles. *Arabian Journal of Chemistry* (in Press) doi:10.1016/j.arabjc.2015.08.028.

Filipkowska, U. (2008). Desorption of reactive dyes from modified chitin. *Environmental Technology 29*, 681-690.

Gad, H.M.H. and El-Sayed, A.A. (2009). Activated carbon from agricultural by-products for the removal of rhodamine-B from aqueous solution. *Journal of Hazardous Materials 168*, 1070-1081.

Ghodake, G., Jadhav, U., Tamboli, D., Kagalkar, A. and Govindwar, S. (2011). Decolorization of textile dyes and degradation of mono-azo dye amaranth by *Acinetobacter calcoaceticus* NCIM 2890. *Indian Journal of Microbiology 51*, 501-508.

Guerrero-Coronilla, I., Morales-Barrera, L., Villegas-Garrido, T.L. and Cristiani-Urbina, E. (2014). Biosorption of amaranth dye from aqueous solution by roots, leaves, stems and the whole plant of *E. crassipes. Environmental Engineering and Management Journal 13*, 1917-1926.

Guerrero-Coronilla, I., Morales-Barrera, L. and Cristiani-Urbina, E. (2015). Kinetic, isotherm and thermodynamic studies of amaranth dye biosorption from aqueous solution onto water hyacinth leaves. *Journal of Environmental Management 152*, 99-108.

Gupta, V.K., Jain, R., Mittal, A., Saleh, T.A., Nayak, A., Agarwal, S. and Sikarwar, S. (2012). Photo-catalytic degradation of toxic dye amaranth on TiO_2/UV in aqueous suspensions. *Materials Science and Engineering: C 32*, 12-17.

Ho, Y.S. and McKay, G. (1999). Comparative sorption kinetics studies of dyes and aromatic compounds onto fly ash. *Journal of Environmental Science and Health, Part A 34*, 1179-1204.

Hossain, M.A., Ngo, H.H., Guo, W.S. and Setiadi, T. (2012). Adsorption and desorption of copper(II) ions onto garden grass. *Bioresource Technology 121*, 386-395.

Lezcano, J.M., González, F., Ballester, A., Blázquez, M.L., Muñoz, J.A. and García-Balboa, C. (2011). Sorption and desorption of Cd, Cu and Pb using biomass from an eutrophized habitat in monometallic and bimetallic systems. *Journal of Environmental Management 92*, 2666-2674.

Mahmoodi, N.M., Hayati, B., Arami, M. and Lan, C. (2011). Adsorption of textile dyes on pine cone from colored wastewater: Kinetic, equilibrium and thermodynamic studies. *Desalination 268*, 117-125.

Rêgo, T.V., Cadaval Jr., T.R.S., Dotto, G.L. and Pinto, L.A.A. (2013). Statistical optimization, interaction analysis and desorption studies for the azo dyes adsorption onto chitosan films. *Journal of Colloid and Interface Science 411*, 27-33.

Shabbir, S., Faheem, M., Ali, N., Kerr, P.G. and Wu, H. (2017). Evaluating role of immobilized periphyton in bioremediation of azo dye

amaranth. *Bioresource Technology 225*, 395-401.

Snehalatha, N., Ravikumar, C., Sekar, N., Jayakumar, V.S. and Joe, J.H. (2008). FT-Raman, IR and UV-visible spectral investigations and *ab initio* computations of a nonlinear food dye amaranth. *Journal of Raman Spectroscopy 39*, 928-936.

Stuart, B. (2004). *Infrared Spectroscopy: Fundamentals and Applications*. John Wiley & Sons.

Szygula, A., Ruiz, M., Guibal, E. and Sastre, A.M. (2008). Removal of an anionic reactive dye by chitosan and its regeneration. *2nd International Conference on Waste Management, Water Pollution, Air Pollution, Indoor Climate*. Corfu, Greece, pp. 24-30.

Volesky, B. (2003). *Sorption and biosorption*. Montreal: Sorbex.

Wambu, E.W., Muthakia, G.K., Shiundu, P.M. and Wa Thiongo, K.J. (2009). Kinetics of copper desorption from regenerated spent bleaching earth. *American-Eurasian Journal of Scientific Research 4(4)*, 317-323.